BNL-215966-2020-JAAM

Long-Range Lamellar Alignment in Diblock Bottlebrush Copolymers via Controlled Oscillatory Shear

B. M. Yavitt, R. Li

To be published in "MACROMOLECULES"

April 2020

Photon Sciences

Brookhaven National Laboratory

U.S. Department of Energy

USDOE Office of Science (SC), Basic Energy Sciences (BES) (SC-22)

DISCLAIMER

Long-Range Lamellar Alignment in Diblock Bottlebrush Copolymers via Controlled Oscillatory Shear

Benjamin M. Yavitt, Huafeng Fei, Gayathri Kopanati, Ruipeng Li, Masafumi Fukuto, H. Henning Winter,* and James J. Watkins*

ABSTRACT: A simple strategy is presented to achieve well-ordered nanostructures in microphase-separated diblock bottlebrush copolymers (dbBB) for potential opportunities in nanotechnology that require large grain sizes and directed orientation. The unique architecture and relaxation processes of dbBBs offer a pathway to enhanced dynamic ordering and reorientation over macroscopic scales. Here, controlled shear is used to align lamellar domains. The high molecular mobility of dbBBs in the melt state, as shown by linear and nonlinear viscoelastic characterization, supports this alignment process. When subjected to large-amplitude oscillatory shear at controlled frequency (ω), strain amplitude (γ), and temperature (T_{shear}), microphase-separated lamellae transition into highly aligned states as determined by small-angle X-ray scattering (SAXS) and transmission electron microscopy (TEM). High throughput synchrotron SAXS is used to rapidly characterize microphase separation and lamellar alignment across the entire bulk sample. Lamellae align parallel to shear planes with an orientation order parameter (S) approaching $S = 0.8$ over a large cubic volume ($V \sim mm^3$).

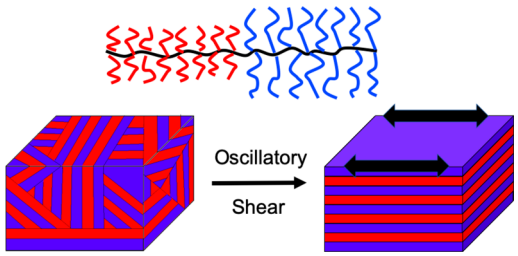

INTRODUCTION

A large effort has been dedicated to the development of macroscopic alignment of block copolymers (BCP), which self-assemble into periodic structures of nanoscale dimensions.[1,2] BCPs generally form local grains, which are internally ordered but are not oriented macroscopically. Long-range order across entire bulk samples is necessary to improve the integral performance of the BCP template for potential use in optical, plasmonic, and energy-harvesting applications.[3−6] Significant work has focused on directing and controlling the macroscopic alignment of BCP domains through mechanical, magnetic, and/or electric fields.[1,2,7−11] Ordering of BCPs of large molecular weight is hindered by chain entanglements that constrain the molecular mobility, contributing to defect formation and limiting grain sizes to order of hundreds of micrometers.[12] Rapid ordering over a large area with large grain sizes (order of mm^2) has remained a challenge when implementing BCP templates for industrial processes.[13]

Alignment by magnetic or electric fields often requires additional additives, such as inorganic NPs or liquid crystals, to induce susceptibility between the microphase-separated domains.[2] Shear alignment is a simple option for aligning BCP systems through the control of processing parameters such as oscillatory shear frequency (ω), operating temperature (T_{shear}), and strain amplitude (γ). Significant theoretical and experimental work has established an understanding of the various mechanisms and stability of aligned morphologies under oscillatory shear.[7,8,14,15] For example, in lamellar forming linear BCPs (LBCP), various cutoff frequencies correspond to the inverse of the characteristic relaxation times ($\tau \sim \omega^{-1}$) of the polymer chains (ω_c) and the global lamellar morphology (ω_d).[8,16,17] Three primary orientations of the lamellae are achieved through controlled large-amplitude oscillatory shearing within the cutoff frequencies: parallel, where the lamellae stack normal to the gradient direction (∇v); perpendicular, where lamellae are normal to the vorticity direction ($\nabla x v$); and transverse, the least stable orientation of lamellae stack normal to the flow direction (v) (Scheme 1).[8]

To increase the chain mobility, most shear alignment is conducted at temperatures near the order-to-disorder transition T_{ODT} ($0.8-1 \cdot T_{ODT}$).[7] In a practical sense, lower operating temperature is more desired for large-scale processing to reduce energy use as well as prevent degradation of susceptible polymers. Large shear strain amplitudes are often applied ($\gamma \sim 100\%$) in the nonlinear regime.[8] Controlled domain alignment with smaller applied shear strain amplitude has been rarely reported but may be desired for certain processing applications or materials with fragile nanostructures.[15]

Scheme 1. Three Potential Orientations of Lamellar Morphology with Respect to Applied Shearing Flow Direction (v)

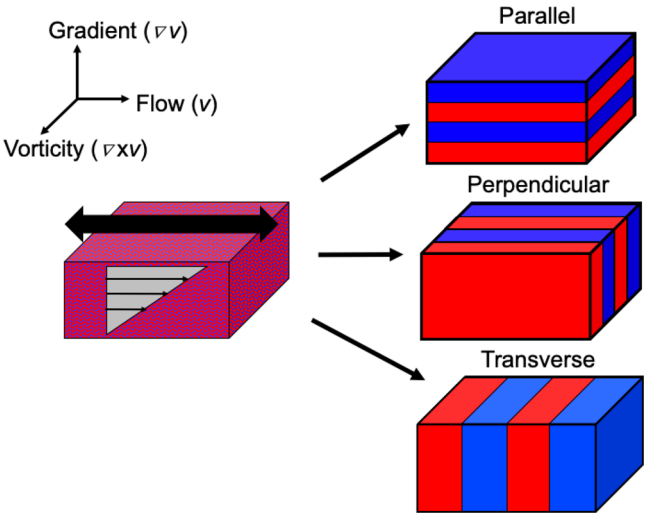

Recently, bottlebrush block copolymers, as an alternative to conventional LBCPs, have shown promise in alleviating the limitations toward rapid ordering over a large sample volume.[13] Specifically, the diblock bottlebrush copolymer (dbBB) rapidly microphase separates and self-organizes into highly ordered states. dbBBs are densely grafted comb polymers with polymeric side chains attached to a linear macromolecular backbone in discrete block segments.[18] Strong steric repulsion from the high grafting density of side chains stretches the dbBB backbone into a wormlike conformation. When coupled with short side chains, the persistence length increases and overall chain entanglements are suppressed.[19,20] The dbBB structure enables fast ordering dynamics (order of minutes) with large domain sizes (d_0 > 100 nm) presenting significant potential in applications for functional materials such as photonic crystals or templating large inorganic nanoparticles (NP) arrays.[13,21−23] Rapid disorder-to-order transitions in lamellar forming polystyrene-*block*-poly(lactide) (PS-*b*-PLA) dbBBs were observed with in situ small-angle X-ray scattering (SAXS) after 30 min of thermal annealing.[21] Song et al. reported the macroscopic self-organization of dbBB and inorganic nanoparticle (NP) composite hybrids with grain sizes at millimeter scale.[13] Despite this achievement of obtaining large volume single grains, fewer efforts have addressed the dbBB alignment process in greater detail.[20,24] Oscillatory shearing of LBCPs is established and can therefore be used as a tool for the potential shear processing of dbBB melts.

In this work, we report the role of oscillatory shear on the orientation of lamellar morphology in a model microphase-separated dbBB, specifically with short side chains and high grafting density. Multiple dynamic regimes and cutoff frequencies are defined by the linear viscoelastic (LVE) response that highlight different modes of relaxation at each characteristic time scale. We relate the impact of controlled oscillatory shearing within each regime to the resulting local and global orientation of the lamellar morphology. Finally, we draw connections to rearrangement mechanisms proposed and discussed in the literature.

EXPERIMENTAL SECTION

Materials. An AB diblock dbBB with brushes of polystyrene-*block*-poly(ethylene oxide) (PS-*b*-PEO) was synthesized by sequential ring-opening metathesis polymerization (ROMP) of norbornene-modified macromonomers (-NB MM) according to established procedures.[13,25] Synthesis details and materials characterization are discussed in the Supporting Information (Schemes S1, S2 and Figures S1, S2). The composition of two blocks is symmetric with equal mass ($f \sim 0.5$). Consideration was taken in the molecular design to keep side chain lengths at low molecular weight (PS-NB MM M_n = 2.9 kg/mol, PEO-NB MM M_n = 5.0 kg/mol) to reduce entanglement probability and maintain high molecular mobility as observed in previous studies.[20]

Sample Preparation. The dbBB samples were prepared by drop-casting from 1.5% (w/v) solutions of dichloromethane (DCM) onto glass substrates, which were covered immediately with glass Petri dishes. After solvent evaporation (∼1 day) and additional drying under nitrogen, the films were removed by a razor blade. The drop-cast films were subsequently melt-pressed into bulk samples for linear and nonlinear viscoelastic characterization by sealing ∼40 mg of material in a circular metal mold sandwiched between pieces of Kapton tape. The samples were annealed under vacuum for 1 h at T = 120 °C, well above the melting temperature of PEO ($T_m \sim 55$ °C) and glass transition temperature of PS blocks ($T_g \sim 100$ °C), and subsequently cooled to room temperature.

Rheology. Viscoelastic measurements were performed on a Malvern Kinexus stress-controlled oscillatory rheometer with an 8 mm parallel plate fixture. The linear viscoelastic response was probed with small-amplitude oscillatory shear (SAOS) frequency sweeps at γ = 1% strain amplitude from T = 80 to 170 °C (PS-*b*-PEO) in increments of ΔT = 10 K over a frequency range of ω = 1−100 rad/s. The time−temperature superposition principle (tTS) was applied to generate a master curve of viscoelastic properties at a reference temperature T_{ref} = 120 °C. Nonlinear viscoelasticity was measured on separately prepared samples by strain sweeps from γ = 0.001−1 at oscillatory frequencies corresponding to various dynamic regimes observed in the linear viscoelastic response. Rheological data were analyzed by using IRIS-RheoHub 2018 software.[26]

Shear Alignment. Shear alignment was conducted in a Linkam CSS 450 optical shearing device by placing approximately 5−10 mg of dbBB on a strip of Kapton tape placed over the optical window (Figure S3a). The dimensions of the bulk sample were approximately 2 mm × 2 mm × 1 mm (V = 4 mm^3). The shearing stage was heated and held at a thermal annealing temperature (1 h at T = 120 °C) to allow microphase separation and self-assembly of lamellar morphology. After thermal annealing, the gap height was set to h = 0.7 mm and the shearing stage temperature was either heated or cooled to T_{shear}, after which controlled oscillatory shear was immediately applied for t = 6 h to ensure adequate time for structure development. After shearing, the stage was cooled to room temperature, and the sample was carefully removed and placed onto a strip of double-sided tape, keeping the sample orientation consistent with the shearing direction (Figure S3b). Because of limitations in the accessible frequency in shear (CSS 450), the apparent shearing frequency was modulated by keeping the applied frequency constant (ω = 1 rad/s) and selecting the corresponding shearing temperature with respect to T_{ref} through the tTS relationship. Shearing conditions are presented in Table 1 for the PS-*b*-PEO dbBB.

Table 1. Shearing Conditions for PS-*b*-PEO as Determined from Linear Viscoelasticity

shearing regime	shearing temp (°C)	freq (rad/s)	strain amplitude (%)	time (h)
high	95	1	50	6
intermediate	115	1	50	6
low	145	1	50	6
static	120			1

Small-Angle X-ray Scattering (SAXS). Scattering measurements were performed at two facilities. Bulk samples were characterized on an in-house Ganesha SAXS-LAB instrument with the Cu Kα 0.154 nm line on the SAXS mode with an approximate beam area of 0.3 × 0.3 mm^2. Each shear aligned sample was oriented in front of the X-ray beam with respect to the three orthogonal directions of the applied shear (gradient, flow, and vorticity) and measured for 10 min. 2-D scattering patterns were collected and integrated into 1-D plots of scattering intensity I vs q. Domain spacings $d = 2\pi/q^*$ were determined from the q^* = primary peak position. 2-D scattering patterns were also azimuthally averaged at q^* into plots of $I(q^*)$ vs azimuthal angle θ (in degrees). Large volume scanning experiments were performed at the Complex Material Scattering (CMS) beamline 11-BM at NSLS-II (Brookhaven National Laboratory). The scattering patterns were collected with a Pilatus 2M detector with a pixel size of 0.172 mm × 0.172 mm with an X-ray wavelength of λ = 0.0918 nm. A silver behenate standard was used for the calibration of all 2-D scattering data. Select shear aligned samples were oriented onto the sample stage along the flow direction and rapidly scanned by SAXS to obtain a map of local orientations. Measurements were taken across the entire top surface of the bulk samples (normal to the gradient direction) and along the edge of the sample (normal to the flow and vorticity directions) with a beam size of 0.1 × 0.1 mm^2 at a step of 0.1 mm (Figure S4). A structural map on the top surface was constructed by a total of 40 × 40 individual SAXS images. The line scan along the edge comprises 40 images. 2-D scattering patterns were processed by integrating into I vs q plots as well as $I(q^*)$ vs θ. The orientation order parameter S was calculated for each 2-D scattering pattern and plotted into order parameter maps. We calculate the orientation order parameter S from the azimuthal plots of q^* as

$$S = \frac{1}{2}(3\langle\cos^2(\theta)\rangle - 1) \quad (1)$$

$$\langle\cos^2(\theta)\rangle = \frac{\int_0^\pi I(\theta)\sin(\theta)\cos^2(\theta)\,d\theta}{\int_0^\pi I(\theta)\sin(\theta)\,d\theta} \quad (2)$$

where θ is the azimuthal angle and $\langle\cos^2(\theta)\rangle$ is the ensemble average of the azimuthal intensity, defined by eq 2.

RESULTS

Linear viscoelastic (LVE) properties of PS-*b*-PEO dbBBs have been reported previously.[27] In the melt state, PS-*b*-PEO is thermorheologically simple and obeys the time−temperature superposition (tTS) principle, and dynamic data can be merged into master curves. Figure 1 shows the dynamic response of PS-*b*-PEO plotted as complex viscosity (η^*/a_T) vs shifted frequency ($a_T\omega$). Shift factors and additional viscoelastic functions are presented in the Supporting Information (Figure S5a,b). The η^* response is partitioned into four distinct scaling regimes, defined by power law scaling $\eta(\omega) \sim \omega^{-x}$.[14] In dbBBs, the different regimes are likely associated with sequential relaxation processes resulting from the highly mobile morphology, facilitated by internal slipping of lamellar domains and the high density of side chain ends in the middle of each layer.[27]

For shear alignment, we wish to apply a large strain amplitude within each regime and investigate the effect of the shearing parameters on lamellar alignment. A single oscillatory frequency is defined at the midpoint of each regime at T_{ref} = 120 °C, designated as low ω ($a_T\omega = 1 \times 10^{-2}$ rad/s), intermediate ω ($a_T\omega = 9 \times 10^0$ rad/s), or high ω ($a_T\omega = 1 \times 10^3$ rad/s). The LVE response at the highest accessible frequencies ($a_T\omega > 10^4$ rad/s) is due to segmental/glassy relaxations and was avoided. The nonlinear viscoelastic response was determined at each ω by strain sweeps. We

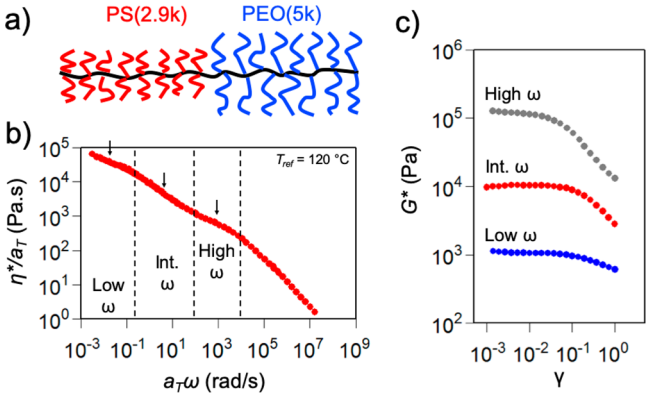

Figure 1. (a) Molecular schematic of densely grafted PS-*b*-PEO dbBB with PS side chain M_n = 2.9 kg/mol and PEO side chain M_n = 5 kg/mol. (b) Linear viscoelasticity represented as complex viscosity (η^*) at reference temperature of T_{ref} = 120 °C. Power law scaling in η^* defines characteristic dynamic regimes: low ω (1×10^{-2} rad/s), intermediate ω (9×10^0 rad/s), and high ω (1×10^3 rad/s). (c) Nonlinear viscoelasticity plotted as G^* vs oscillatory shear strain amplitude (γ) at selected frequencies (ω) within each dynamic regime.

define the extent of the LVE regime at strain amplitudes up to the drop-off in G^*. The LVE regime extends up to $\gamma \sim 10\%$ at low ω, while at high ω the LVE regime extends to $\gamma \sim 2$−3%, and the drop-off in G^* is the most drastic. The parameters for shear alignment were selected according to the analysis of the linear and nonlinear viscoelastic characterization (Table 1). The applied strain was selected as γ = 50%, well within the nonlinear viscoelastic regime for all selected shearing frequencies.

After sufficient shear alignment processing, the microphase segregation, morphology, and grain structure were investigated with SAXS. Figure 2 shows reconstructions of 2-D scattering patterns collected along orthogonal directions with respect to the applied shear (gradient (∇v), flow (v), and vorticity ($\nabla x v$)). In all directions, microphase segregation is identified by diffraction rings corresponding to the strong primary peak q^* in 1-D SAXS spectra (Figure S6). Lamellar morphology is determined by identification of higher order peaks at a ratio of q^*:2q^*:3q^*. The orientation of the lamellae through the bulk sample is described by the anisotropy in the 2-D scattering patterns. In the PS-*b*-PEO control sample under no shearing (static), isotropic patterns in all three directions indicate no preferred orientation of the structure (Figure 2a). After high ω shearing, the diffraction pattern is also isotropic like the static condition. The absolute intensity of q^* in the 1-D spectra is much lower compared to other shearing conditions, and the higher order scattering peaks intensities are much weaker (Figure S6b). The scattering patterns begin to express anisotropy after intermediate and low ω shearing (Figure 2c,d). Twofold symmetric scattering patterns emerge at the low ω condition in all three directions. In the gradient direction of Figure 2d, the ring is weak and diffuse, while in the flow and vorticity directions, the pair of high-intensity spots are strong. The reconstruction of the scattering pattering in three orthogonal directions suggests parallel alignment of the lamellar domains, where the layers arrange in the flow direction, stacked normal to the gradient direction. Electron microscopy images of cryomicrotomed sections along the flow direction of the low ω shear aligned sample show exceptional

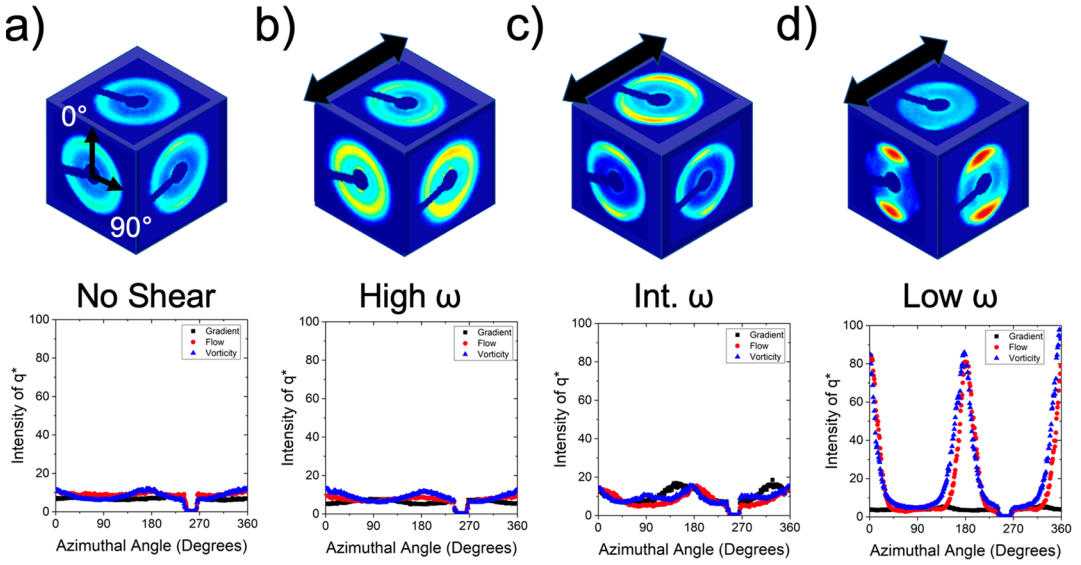

Figure 2. 2-D SAXS patterns and corresponding azimuthal integration of primary scattering peak q^* of microphase-segregated morphology in three orthogonal directions for PS-*b*-PEO after (a) thermal annealing under static conditions as well as shearing at (b) high ω (c) intermediate ω and (d) low ω. 2-D images scaled to standardized intensity scale. Black arrows designate the flow direction (v) on the top shearing surface.

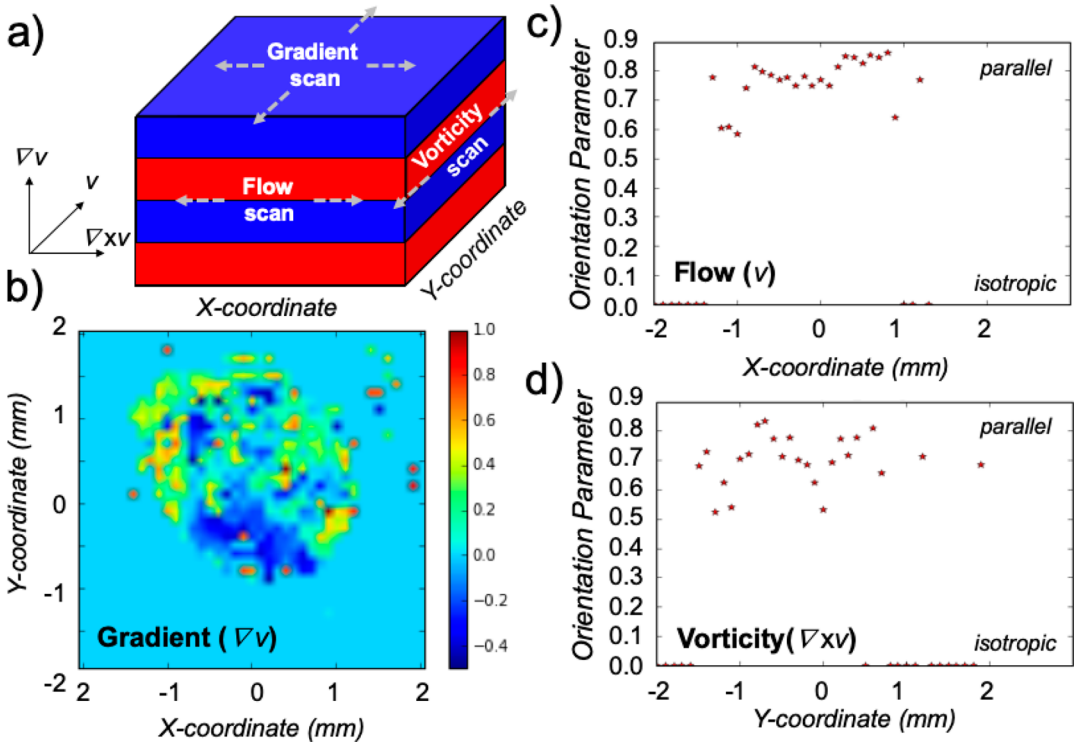

Figure 3. (a) Schematic of SAXS scanning technique across each orthogonal face of the bulk shear aligned dbBB samples. The orientation order parameter S is plotted across each direction in subsequent figures. (b) 2-D map of S compiled from 2-D scattering patterns at each location along the gradient scan (∇v). (c) Orientation order parameter S along the edge of the sample in the flow plane (v). S is consistently ~0.8 along entire edge of almost 2 mm. (d) Orientation order parameter S along the edge of the sample in the vorticity plane (∇xv). S is ~0.7−0.8 along entire edge of almost 2 mm. Strong orientation in flow and vorticity plane suggests alignment of lamellae parallel to applied shear.

alignment of the lamellar domains (Figure S7). The intermediate ω also has intense scattering rings in the flow and vorticity directions; however, the anisotropy is not as prevalent, and there is significant intensity in the gradient direction as well.

The azimuthal angular dependence of q^* is also plotted in Figure 2 to quantitatively visualize the anisotropy in the 2-D scattering patterns. The most drastic intensity in the azimuthal plots is clearly in the low ω regime, where the peak intensity is centered on azimuthal angle $\theta = 0°$ and 180°, highlighting the 2-fold symmetric pattern.

The 2-D SAXS patterns and azimuthal line cuts of q^* suggest that oscillatory shear either induces or enhances the collective orientation of the lamellar grain structure and that the strongest effect is observed after low ω oscillation. We investigate the impact of low ω shear on the global/macroscale

orientation with synchrotron SAXS characterizations. The orientation order parameter S is calculated for each 2-D scattering pattern and plotted into order parameter maps encompassing the entire sample volume in the gradient, flow, and vorticity directions (Figure 3). S is commonly used to determine order in liquid crystals, block copolymers, and other oriented nanoscale materials, accounting for orientation over all three dimensions.[28] Here, S ranges from $S = -0.5$ to 1 according to the orientation of the 2-D pattern, where $\theta = 0°$ is vertical up, and θ increases clockwise (full formulism in the Supporting Information). $S = 0$ is isotropic orientation. The axis of the reference direction ($\theta = 0°$) for the calculation of S differs between Figure 3b and Figure 3c,d. For those scattering patterns represented in Figure 3b, the reference axis is the flow direction (v), where a value of $S = 1$ corresponds to transverse lamellar orientation and $S = -0.5$ is a perpendicular orientation. For Figure 3c,d, the reference axis is the gradient direction (∇v). In such an orientation, $S = 1$ would correspond to parallel lamellar orientation, and $S = -0.5$ is either the perpendicular orientation for Figure 3c or the transverse orientation for Figure 3d. The scan window of SAXS measurements is much larger than the sample dimensions. Therefore, in the remaining space of the plots where there is no signal from the sample, $S = 0$ is observed.

The limits of alignment must be considered in all three directions to fully resolve the macroscale orientation and alignment. The surface orthogonal to the gradient direction presented in Figure 3b is generally isotropic and S is close to zero (between $S = -0.2$ and 0.2), suggesting poor orientation of the lamellae in that direction. Plots of S along the flow and vorticity surfaces (Figures 3c and 3d, respectively) show increased order with value of $S = 0.7-0.8$ over the entire 2 mm sample length, suggesting strong "parallel" alignment over an exceptionally large volume. The observation of scattering intensity and alignment in the gradient direction suggests that there may be small populations of grains not fully aligned in the parallel orientation, possibly due to local edge effects which are observed over such a large macroscopic volume. Overall, the analysis in each orthogonal direction confirms that the lamellae are still "highly aligned" in a parallel orientation.

Large volume synchrotron SAXS analysis of additional samples reveals the impact of the shear compared to thermal annealing under static conditions (Figures S8 and S9). The thermally annealed sample in Figure 2a (1 h at $T = 120$ °C) represents the initial condition before shearing and exhibits significantly large grains with $S = 0.4$ and $S = -0.2$ in the gradient plane, suggesting the global morphology is not uniformly aligned. S fluctuates significantly along the entire edge of the sample, suggesting there are some areas of orientation, but the grain size is small and not well aligned. An additional sample was thermally annealed at $T = 145$ °C for 6 h (the same thermal conditions as the low ω regime) but in the absence of shear to elucidate the effect of higher thermal annealing temperature exclusively (Figure S9). While S increases significantly along the flow and vorticity directions, there are large oriented grains visible in the gradient direction, suggesting that the lamellae are not completely aligned into the parallel orientation as they are when shear is applied.

DISCUSSION

There are various pathways proposed for lamellar orientation in classical LBCP systems explained through experimental morphology characterization as well as advanced in situ techniques.[7,8,14,15,29,30] Here, we focus on the low ω regime, as this produced the strongest alignment in the dbBBs. It is understood that low ω oscillations target the slowest relaxation processes.[7] Koppi et al. proposed that nanostructure align through a "defect mediated" stress relaxation process, where defects in the long-range order become the stress bearing structures that respond on the longest time scales.[7] For example, lamellar defects present in an isotropic, quenched BCP will reorder after shearing, resulting in parallel alignment of the lamellae. The defect driven mechanism is plausible for the PS-*b*-PEO dbBB system, which is globally isotropic after static thermal annealing according to Figure 2a. The melt state morphology present during shear processing was previously determined to contain such long-range defects.[27] The long-range lamellar arrangement of the PS and PEO domains is difficult to characterize in the melt state due to the decrease in scattering contrast with increasing temperature. However, the characteristic q position of the primary scattering peak is independent of temperature, suggesting the two domains are still microphase separated and the PS−PEO interface is maintained. The rearrangement of domains is likely enhanced by the presence of confined internal sliding layers resulting from high density of unentangled side chains within the domains.[27] The backbone conformation driven by the inherent stiffness of the poly(norbornene) backbone and the steric repulsion in the densely grafted side chains contribute to the reduced entanglements. The backbone conformation is interrogated through the relationship between lamellar spacing d_0 and backbone contour length $L = N_{bb}L_0$, where N_{bb} is the backbone degree of polymerization and L_0 is the length of one macromonomer repeat unit ($L_0 = 0.62$ nm) according to Dalsin et al.[31] In a fully extended, bilayer lamellar arrangement, $d_0 = 2L$. However, we find that $d_0 < 2L$ (see the Supporting Information), suggesting the backbone likely retains some degree of flexibility in the microphase-separated state, consistent with recent literature reports.[32,33] The resulting lack of entanglements reduces topological constraints commonly found within complementary entangled LBCPs and facilitates rapid rearrangement and relaxation of the global structure at low ω. The internal layers act as an additional interface within the microphase-separated structure (either a PS−PS or PEO−PEO interface) that likely responds to the shear flow. Higher ω oscillations target these faster internal domain relaxation processes, which are not correlated in the melt state and therefore do not produce the globally aligned structures. Hard body grain rotation is also widely accepted as a route to parallel aligned domains.[7] However, the rotation mechanism is highly unlikely in the dbBBs as the "hard body" grain structure is weakly defined in the melt state.

As presented, the characterizations are entirely ex situ representations of the structure and morphology. While orientation mechanisms may be proposed and discussed according to material states before and after shearing, direct in situ measurements are desired to quantitatively investigate the onset and evolution of lamellar orientation. In situ measurements are especially crucial for this dbBB system as the melt state structure is different than the structure at room temperature characterized ex situ. Additional development of in situ Rheo/SAXS synchrotron techniques is necessary to fully investigate such time-resolved evolution of structure during shear processing. The ability to measure dynamic data (G' and G'') while performing Rheo/SAXS measurements is also desired. It is well-known that the viscoelastic response of

aligned BCP structures is dependent on the orientation.[11,30] As a result, the onset and existence of unique orientations and metastable states could be identified before, during, and after shear processing.

The demonstration of shear-induced alignment in the dbBB materials is interesting and especially appealing for implementation in future processing applications. As previously stated, the controlled domain ordering at low temperature ($T_g < T \ll T_{ODT}$) is advantageous and achieved with the dbBB architecture. This provides an expanded regime of potential processing conditions for the controlled assembly of dbBB domains via shear. Advantages of reducing the processing temperature include speeding up processing time, reducing the energy use, and reducing the chance of sample degradation. The exceptionally large volume alignment (on order of $V = mm^3$) is confirmed and characterized by our synchrotron SAXS techniques and measurements. These highlights all convey the potential for dbBB implementation in applications where nanoscale domain alignment must be easily and efficiently controlled.

CONCLUSION

In summary, we build upon the unique macroscopic ordering achieved in microphase-separated dbBBs and demonstrate the ability to control that alignment by using oscillatory shear techniques. Long-range order was maintained over an exceptionally large sample area as described by high throughput small-angle X-ray scattering characterization. The layer orientation and strength of orientation were established by the orientation order parameter S. The orientation was attributed to the elimination of lamellar defects, facilitated by the high mobility of the microphase structure in the melt state. The simple strategy for the long-range alignment applies to a wide range of potential functional materials and applications and invites the manipulation of composite materials containing small molecules, quantum dots, anisotropic NPs, magnetic NPs, and so on. The well-aligned NP arrays may serve as templates for the fabrication of high-performance plasmonic devices or optical materials. The ultrafast kinetics of dbBB ordering offers new opportunities for efficient, low-energy, and scalable processes.

AUTHOR INFORMATION

Corresponding Authors

James J. Watkins − *Department of Polymer Science and Engineering, University of Massachusetts Amherst, Amherst, Massachusetts 01003, United States*; Email: watkins@polysci.umass.edu

H. Henning Winter − *Department of Polymer Science and Engineering and Department of Chemical Engineering, University of Massachusetts Amherst, Amherst, Massachusetts 01003, United States*; orcid.org/0000-0002-5470-7736; Email: winter@engin.umass.edu

Authors

Benjamin M. Yavitt − *Department of Polymer Science and Engineering, University of Massachusetts Amherst, Amherst, Massachusetts 01003, United States*; orcid.org/0000-0001-9308-7472

Huafeng Fei − *Department of Polymer Science and Engineering, University of Massachusetts Amherst, Amherst, Massachusetts 01003, United States*; orcid.org/0000-0002-9983-2725

Gayathri Kopanati − *Department of Polymer Science and Engineering, University of Massachusetts Amherst, Amherst, Massachusetts 01003, United States*

Ruipeng Li − *National Synchrotron Light Source II, Brookhaven National Laboratory, Upton, New York 11973, United States*

Masafumi Fukuto − *National Synchrotron Light Source II, Brookhaven National Laboratory, Upton, New York 11973, United States*

ACKNOWLEDGMENTS

This work is supported by the NSF Center for Hierarchical Manufacturing at the University of Massachusetts Amherst (CMMI-1025020) and ACS-PRF (58675-ND10). The Materials Research Science and Engineering Center at University of Massachusetts Amherst supported facilities used in this work. Small-angle X-ray scattering was conducted on the CMS beamline (11-BM) of the National Synchrotron Light Source II, a U.S. Department of Energy (DOE) Office of Science User Facility operated for the DOE Office of Science by Brookhaven National Laboratory under Contract DE-SC0012704. Special thanks to Dr. Yue Gai and Prof. Dong-Po Song for early discussions on bottlebrush block copolymer shear alignment.

REFERENCES

(1) Hu, H.; Gopinadhan, M.; Osuji, C. O. Directed Self-Assembly of Block Copolymers: A Tutorial Review of Strategies for Enabling Nanotechnology with Soft Matter. *Soft Matter* **2014**, *10* (22), 3867−3889.

(2) Darling, S. B. Directing the Self-Assembly of Block Copolymers. *Prog. Polym. Sci.* **2007**, *32* (10), 1152−1204.

(3) Bates, C. M.; Bates, F. S. 50th Anniversary Perspective: Block Polymers—Pure Potential. *Macromolecules* **2017**, *50* (1), 3−22.

(4) Rancatore, B. J.; Mauldin, C. E.; Tung, S.-H.; Wang, C.; Hexemer, A.; Strzalka, J.; Fréchet, J. M. J.; Xu, T. Nanostructured Organic Semiconductors via Directed Supramolecular Assembly. *ACS Nano* **2010**, *4* (5), 2721−2729.

(5) Kao, J.; Thorkelsson, K.; Bai, P.; Rancatore, B. J.; Xu, T. Toward Functional Nanocomposites: Taking the Best of Nanoparticles, Polymers, and Small Molecules. *Chem. Soc. Rev.* **2013**, *42* (7), 2654−2678.

(6) Yoon, J.; Lee, W.; Thomas, E. L. Thermochromic Block Copolymer Photonic Gel. *Macromolecules* **2008**, *41* (13), 4582−4584.

(7) Koppi, K. A.; Tirrell, M.; Bates, F. S.; Almdal, K.; Colby, R. H. Lamellae Orientation in Dynamically Sheared Diblock Copolymer Melts. *J. Phys. II* **1992**, *2*, 1941−1959.

(8) Chen, Z.-R.; Kornfield, J. A. Flow-Induced Alignment of Lamellar Block Copolymer Melts. *Polymer* **1998**, *39* (19), 4679−4699.

(9) Ruppel, M.; Pester, C. W.; Langner, K. M.; Sevink, G. J. A.; Schoberth, H. G.; Schmidt, K.; Urban, V. S.; Mays, J. W.; Böker, A. Electric Field Induced Selective Disordering in Lamellar Block Copolymers. *ACS Nano* **2013**, *7* (5), 3854−3867.
(10) Gopinadhan, M.; Choo, Y.; Kawabata, K.; Kaufman, G.; Feng, X.; Di, X.; Rokhlenko, Y.; Mahajan, L. H.; Ndaya, D.; Kasi, R. M.; et al. Controlling Orientational Order in Block Copolymers Using Low-Intensity Magnetic Fields. *Proc. Natl. Acad. Sci. U. S. A.* **2017**, *114* (45), E9437−E9444.
(11) Scott, D. B.; Waddon, A. J.; Lin, Y. G.; Karasz, F. E.; Winter, H. H. Shear-Induced Orientation Transitions in Triblock Copolymer Styrene-Butadiene-Styrene with Cylindrical Domain Morphology. *Macromolecules* **1992**, *25* (16), 4175−4181.
(12) Ryu, H. J.; Fortner, D. B.; Lee, S.; Ferebee, R.; De Graef, M.; Misichronis, K.; Avgeropoulos, A.; Bockstaller, M. R. Role of Grain Boundary Defects during Grain Coarsening of Lamellar Block Copolymers. *Macromolecules* **2013**, *46* (1), 204−215.
(13) Song, D.-P.; Li, C.; Colella, N. S.; Xie, W.; Li, S.; Lu, X.; Gido, S. P.; Lee, J.-H.; Watkins, J. J. Large-Volume Self-Organization of Polymer/Nanoparticle Hybrids with Millimeter-Scale Grain Sizes Using Brush Block Copolymers. *J. Am. Chem. Soc.* **2015**, *137*, 12510−12513.
(14) Wiesner, U. B. Lamellar Diblock Copolymers under Large Amplitude Oscillatory Shear Flow: Order and Dynamics. *Macromol. Chem. Phys.* **1997**, *198* (11), 3319−3352.
(15) Winey, K. I.; Patel, S. S.; Larson, R. G.; Watanabe, H. Interdependence of Shear Deformations and Block Copolymer Morphology. *Macromolecules* **1993**, *26*, 2542−2549.
(16) Gupta, V. K.; Krishnamoorti, R.; Chen, Z.-R.; Kornfield, J. A.; Smith, S. D.; Satkowski, M. M.; Grothaus, J. T. Dynamics of Shear Alignment in a Lamellar Diblock Copolymer: Interplay of Frequency, Strain Amplitude, and Temperature. *Macromolecules* **1996**, *29* (3), 875−884.
(17) Chen, Z.-R.; Kornfield, J. A.; Smith, S. D.; Grothaus, J. T.; Satkowski, M. M. Pathways to Macroscale Order in Nanostructured Block Copolymers. *Science (Washington, DC, U. S.)* **1997**, *277* (5330), 1248−1253.
(18) Verduzco, R.; Li, X.; Pesek, S. L.; Stein, G. E. Structure, Function, Self-Assembly, and Applications of Bottlebrush Copolymers. *Chem. Soc. Rev.* **2015**, *44*, 2405−2420.
(19) Dalsin, S. J.; Hillmyer, M. A.; Bates, F. S. Linear Rheology of Polyolefin-Based Bottlebrush Polymers. *Macromolecules* **2015**, *48*, 4680−4691.
(20) Yavitt, B. M.; Gai, Y.; Song, D.-P.; Winter, H. H.; Watkins, J. J. High Molecular Mobility and Viscoelasticity of Microphase-Separated Bottlebrush Diblock Copolymer Melts. *Macromolecules* **2017**, *50* (1), 396−405.
(21) Gu, W.; Huh, J.; Hong, S. W.; Sveinbjornsson, B. R.; Park, C.; Grubbs, R. H.; Russell, T. P. Self-Assembly of Symmetric Brush Diblock Copolymers. *ACS Nano* **2013**, *7* (3), 2551−2558.
(22) Song, D.-P.; Lin, Y.; Gai, Y.; Colella, N. S.; Li, C.; Liu, X.-H.; Gido, S. P.; Watkins, J. J. Controlled Supramolecular Self-Assembly of Large Nanoparticles in Amphiphilic Brush Block Copolymers. *J. Am. Chem. Soc.* **2015**, *137* (11), 3771−3774.
(23) Liberman-Martin, A. L.; Chu, C. K.; Grubbs, R. H. Application of Bottlebrush Block Copolymers as Photonic Crystals. *Macromol. Rapid Commun.* **2017**, *38*, 1700058.
(24) Choo, Y.; Mahajan, L. H.; Gopinadhan, M.; Ndaya, D.; Deshmukh, P.; Kasi, R. M.; Osuji, C. O. Phase Behavior of Polylactide-Based Liquid Crystalline Brushlike Block Copolymers. *Macromolecules* **2015**, *48*, 8315−8322.
(25) Gai, Y.; Song, D.-P.; Yavitt, B. M.; Watkins, J. J. Polystyrene-Block -Poly(Ethylene Oxide) Bottlebrush Block Copolymer Morphology Transitions: Influence of Side Chain Length and Volume Fraction. *Macromolecules* **2017**, *50*, 1503−1511.
(26) Winter, H. H.; Mours, M. The Cyber Infrastructure Initiative for Rheology. *Rheol. Acta* **2006**, *45* (4), 331−338.
(27) Yavitt, B. M.; Fei, H.-F.; Kopanati, G. N.; Winter, H. H.; Watkins, J. J. Power Law Relaxations in Lamellae Forming Brush Block Copolymers with Asymmetric Molecular Shape. *Macromolecules* **2019**, *52* (4), 1557−1566.
(28) Zhang, C.; Cavicchi, K. A.; Li, R.; Yager, K. G.; Fukuto, M.; Vogt, B. D. Thickness Limit for Alignment of Block Copolymer Films Using Solvent Vapor Annealing with Shear. *Macromolecules* **2018**, *51*, 4213.
(29) Kannan, R. M.; Kornfield, J. A. Evolution of Microstructure and Viscoelasticity during Flow Alignment of a Lamellar Diblock Copolymer. *Macromolecules* **1994**, *27* (5), 1177−1186.
(30) Gupta, V. K.; Krishnamoorti, R.; Kornfield, J. A.; Smith, S. D. Evolution of Microstructure during Shear Alignment in a Polystyrene-Polyisoprene Lamellar Diblock Copolymer. *Macromolecules* **1995**, *28* (13), 4464−4474.
(31) Dalsin, S. J.; Rions-maehren, T. G.; Beam, M. D.; Bates, F. S.; Hillmyer, M. A.; Matsen, M. W. Bottlebrush Block Polymers: Quantitative Theory and Experiments. *ACS Nano* **2015**, *9* (12), 12233−12245.
(32) Fei, H.-F.; Yavitt, B. M.; Hu, X.; Kopanati, G.; Ribbe, A.; Watkins, J. J. Influence of Molecular Architecture and Chain Flexibility on the Phase Map of Polystyrene- Block -Poly-(Dimethylsiloxane) Brush Block Copolymers. *Macromolecules* **2019**, *52* (17), 6449−6457.
(33) Sunday, D. F.; Chang, A. B.; Liman, C. D.; Gann, E.; DeLongchamp, D. M.; Thomsen, L.; Matsen, M. W.; Grubbs, R. H.; Soles, C. L. Self-Assembly of ABC Bottlebrush Triblock Terpolymers with Evidence for Looped Backbone Conformations. *Macromolecules* **2018**, *51* (18), 7178−7185.